Soil-atmosphere exchange flux of total gaseous mercury (TGM) at subtropical and temperate forest catchments

Jun Zhou [a, b, c, f], Zhangwei Wang [a, c, *], Xiaoshan Zhang [a, c], Charles T. Driscoll [d], Che-Jen Lin [e]

a. State Key Laboratory of Urban and Regional Ecology, Research Center for Eco-Environmental Sciences, Chinese Academy of Sciences, Beijing 100085, China.

b. Key Laboratory of Soil Environment and Pollution Remediation, Institute of Soil Science, Chinese Academy of Sciences, Nanjing 210008, China.

c. University of Chinese Academy of Sciences, Beijing 100049, China.

d. Department of Civil and Environmental Engineering, Syracuse University, 151 Link Hall, Syracuse, New York 13244, United States.

e. Center for Advances in Water and Air Quality, Lamar University, Beaumont, Texas 77710, United States.

f. Department of Environmental, Earth and Atmospheric Sciences, University of Massachusetts, Lowell, 01854, USA

* Corresponding author: Zhangwei Wang

E-mail address: wangzhw@rcees.ac.cn (Z. Wang); Phone: +86 10 62849168.

No.18 Shuangqing Road, Beijing 100085, China

First author e-mail: zhoujun@issas.ac.cn (J. Zhou); Phone: +86 25 86881319.

No.73 East Beijing Road, Nanjing 210008, China.

Abstract: Evasion from soil is the largest source of mercury (Hg) to the atmosphere from terrestrial ecosystems. To improve understanding of controls and in estimates of forest soil-atmosphere fluxes of total gaseous Hg (TGM), measurements were made using dynamic flux chambers (DFC) over 130 and 96 days for each of five plots at a subtropical forest and a temperate forest, respectively. At the subtropical forest the highest net soil Hg emissions were observed for an open field (24 ± 33 ng m^{-2} hr^{-1}), followed by two coniferous forest plots (2.8 ± 3.9 and 3.5 ± 4.2 ng m^{-2} hr^{-1}), broad-leaved forest plot (0.18 ± 4.3 ng m^{-2} hr^{-1}), and the remaining wetland site showing net deposition (−0.80 ± 5.1 ng m^{-2} hr^{-1}). At the temperate forest, the highest fluxes and net soil Hg emissions were observed for a wetland (3.81 ± 0.52 ng m^{-2} hr^{-1}) and an open field (1.82 ± 0.79 ng m^{-2} hr^{-1}), with lesser emission rates in deciduous broad-leaved forest (0.68 ± 1.01 ng m^{-2} hr^{-1}) and deciduous needle-leaved forest (0.32 ± 0.96 ng m^{-2} hr^{-1}) plots, and net deposition at an evergreen pine forest (−0.04 ± 0.81 ng m^{-2} h^{-1}). High solar radiation and temperature during summer resulted in the high Hg emissions in the subtropical forest, and the open field and evergreen pine forest at the temperate forest. At the temperate deciduous plots, the highest Hg emission occurred in spring during leaf-off period due to direct solar radiation exposure to soils. Fluxes showed strong positive relationships with solar radiation and soil temperature, and negative correlations with ambient-air TGM concentration in both subtropical and temperate forests, with area-weighted compensation points of 6.82 and 3.42 ng m^{-3}, respectively. The values of the compensation points suggest that the atmospheric TGM concentration can play a critical role in limiting TGM emissions from the forest floor. Climate change and land-use disturbance may increase the compensation points in both temperate and subtropical forests. Future research should focus on the role of legacy soil Hg in reemissions to the atmosphere as decreases in primary emissions drive decreases in TGM concentrations and disturbance of climate change and land use.

Keywords: soil-air flux of total gaseous mercury; dynamic flux chamber; compensation point; climate change; land use

1. Introduction

Mercury (Hg) is a persistent, bio-accumulative, toxic and well-established global contaminant (Obrist et al., 2018). Unlike other trace metals in the atmosphere, the Hg mainly exists as gaseous elemental Hg (Hg(0)), which accounts more than 90% of total gaseous Hg (TGM). Hg(0) is relatively inert and has a long atmospheric lifetime of 0.5–1 year, which allows for long range transport (Kamp et al., 2018;Slemr et al., 2018;St Louis et al., 2019). Global long-range atmospheric transport and deposition is the main pathway of Hg input to remote ecosystems (Lin et al., 2019;Ly Sy Phu et al., 2019;Sun et al., 2019). Soils account for more than 90% of Hg stored in terrestrial ecosystems (Obrist, 2012), with global top soil Hg pools (0–40 cm) estimated at > 300 000 Mg (Hararuk et al., 2013;Zhou et al., 2017a). The large soil Hg pools not only stem from geologic sources, but also from a legacy of historically anthropogenic emissions over the centuries (Obrist et al., 2014;Du et al., 2019).

Although many studies have focused on primary anthropogenic Hg emissions, releases from natural source materials is also an important pathway but with greater uncertainty and variability, including emissions from natural reservoirs (e.g. volcanic activity, geothermal sources, weathering of Hg from soil minerals) and re-emissions of previous deposited Hg. These natural sources can be equal to or two-fold larger than anthropogenic sources (Outridge et al., 2018;Fraser et al., 2018). Recent global Hg models estimate that 3600 Mg yr^{-1} of atmospheric Hg is deposited to terrestrial surfaces, with 1000 Mg yr^{-1} re-emitted back to the atmosphere (Outridge et al., 2018). Moreover, compared to primary anthropogenic emissions of Hg (2500 Mg yr^{-1}), estimates of re-emissions from soil surfaces are highly uncertain (Outridge et al., 2018;Wang et al., 2018). Compiling data from 132 studies, Agnan et al. (2016) found that the Earth's surface (particularly in East Asia) is an increasingly important source of total gaseous Hg (TGM) emissions, with up to half of the global emissions derived from natural sources. They estimated terrestrial TGM emissions of 607 Mg yr^{-1}, but with a large uncertainty range of −513 to 1353 Mg yr^{-1}. Additionally, a recent review suggests that future research should focus on campaigns to understand forest Hg behavior and long-term Hg observations, particularly in Asia (Zhang et al., 2019b).

Forest soils receive Hg inputs from: 1) throughfall that include wet deposition plus the wash off of Hg (II) deposited on foliage surfaces; 2) litterfall that contains foliage and other plant materials that have assimilated atmospheric Hg(0); and 3) direct dry Hg deposition to soil from the atmosphere

(Teixeira et al., 2018;Risch et al., 2017;Olson et al., 2018;Cheng et al., 2020). Mercury outputs from forest soils occur from surface or subsurface runoff and air-land surface evasion. Forest soils are highly complex media, with important features that affect soil-air exchange, including soil physio-chemical characteristics (e.g., porosity, oxygen availability, redox potential, organic matter, pH) (Obrist et al., 2010;Carpi et al., 2014). Other factors also influence this process, such as meteorological conditions (e.g., solar radiation, air temperature, precipitation) (Zhou et al., 2015;O'Connor et al., 2019), atmospheric chemistry (ozone, nitrate and hydroxyl radicals) (Peleg et al., 2015;Angot et al., 2016), atmospheric TGM concentrations (Wang et al., 2007) and biological processes (Obrist et al., 2010;Chen et al., 2017). Therefore, to characterize and quantify land-atmosphere exchange of TGM, it is necessary to understand the roles of these factors in mediating this process.

Field studies have shown that elevated anthropogenic Hg emissions in South-East Asia have resulted high atmospheric Hg concentrations an deposition regionally (Kumari et al., 2015;Pan et al., 2010;Zhang et al., 2019b). Forests experience particularly elevated net Hg loads due to enhanced deposition associated with the tree canopy, especially in China (Wang et al., 2016;Zhang et al., 2019a). The annual loading of THg to subtropical forests in China have been shown to be much higher than forest catchments in Europe and North America (Wright et al., 2016;Zhou et al., 2020). High Hg deposition has resulted in elevated soil Hg pools in Chinese subtropical forests (Wang et al., 2018;Wang et al., 2009). In contrast, a recent study showed that the Hg deposition and soil Hg concentrations at a temperate forest in China were similar to those in Europe and North America (Zhou et al., 2020). The forested area in China is 2.2×10^4 km^2, with about 50% and 40% occurring in subtropical and temperate zones, respectively. Therefore, it seems likely that subtropical and temperate forests in China, with contrasting climate, vegetation cover, and atmospheric Hg deposition, may also show different patterns of Hg cycling.

Forest ecosystems not only act as sinks for atmospheric Hg deposition, but can also serve as sources resulting from legacy Hg that has accumulated in surface soil. For example, one study constructed the Hg budget in subtropical forest in southern China showing that the forest is a minor sink for atmospheric Hg but a significant net Hg(0) source (58.5 $\mu g\ m^{-2}\ yr^{-1}$) (Yu et al., 2020). In contrast, another study also in southern China using budgets of air-foliage and air-soil Hg(0) exchange fluxes, showed that forest is a net sink of Hg(0) (20.1 $\mu g\ m^{-2}\ yr^{-1}$) (Yuan et al., 2019a;Yuan

et al., 2019b). These results indicate that there is considerable uncertainty and variability in the source-sink behavior of Hg in subtropical forests of southern China. Furthermore, no studies have conducted in northern China to characterize the Hg fluxes in the temperate forest.

There has been much research characterizing Hg fluxes between the forest floor and the atmosphere from studies worldwide, as reviewed by Zhu et al. (2016) and Agnan et al. (2016). In this paper, we present measurements on atmosphere-land Hg fluxes conducted over 130-days and 96-days, respectively, during four seasons for five sites both at a temperate forest catchment at Mt. Dongling (MDL) and a subtropical forest catchment at Tieshanping Forest Park (TFP) in China. The aims of this investigation were to (1) characterize the air-land surface Hg fluxes in different terrestrial ecosystems; (2) conduct detailed field measurements to characterize the uncertainty of land use and climate change in air-surface fluxes of TGM in forest catchments; and (3) to compare estimates of Hg emissions from forest soils at temperate and subtropical zones. We hypothesize that a multi-plot and multi-seasonal study of soil-air fluxes in each forest system will provide new perspectives on the climate change and land use on the soil-air Hg fluxes, and improve understanding and estimates of soil Hg evasion from forest ecosystems.

2. Materials and methods

2.1. Study area

This study was conducted at TFP in the subtropical zone (106°41.24′E, 29°37.42′N) and at MDL in the temperate zone (115°26′, E40°00' N) in China (Fig. 1). The TFP is dominated by a Masson pine (*Pinus massoniana* Lamb.) stand (conifer) with some associated species, such as camphor (*Cinnamom camphora*) and Gugertree (*Schima superba* Gardn), which were planted in 1960s following the loss of a natural Masson pine forest. The forest is located about 20 km northeast of Chongqing City, at an altitude from 200 to 550 m. The mean annual precipitation is 1028 mm, with 75% of the rainfall occurring from May to October. The mean annual air temperature is 18.2 ℃. The total area of the study forest in the TFP is 1.06×10^3 ha. The soil is typically mountain yellow earth (corresponding to an Acrisol in the FAO) (FAO, 1988), with clay mineralogy dominated by kaolinite (Zhou et al., 2016).

Mt. Dongling is near the Beijing Forest Ecosystem Research Station, Chinese Academy of Sciences, which is located 110 km southwest of mega-city Beijing in North China. The elevation is

1300 m asl. The annual average rainfall is 612 mm and mean relative humidity is 66%. The climate of the region is predominantly warm temperate continent monsoon with an annual average temperature of 4.8 °C and precipitation of 611.9 mm. Soil type is mountain brown earth (corresponding to a Eutric cambisol in FAO) (FAO, 1988) (Zhou et al., 2018). The relatively cool climate in the study area has resulted in deep litter and high organic matter concentrations (Fang et al., 2007). The study area is a mature, secondary forest protected since the 1950s following the extensive deforestation. Hg concentrations in environmental media at the site are provided in the Supporting Information (SI, Supporting Text).

2.2. Dynamic flux chamber (DFC) measurement

To reduce the spatial uncertainty in Hg fluxes, different ecosystems were selected for study in a sub-catchment at the subtropical TFP, including a coniferous forest (plots S-A and S-B), a wetland (plot S-C), a broad-leaved (camphor) forest (plot S-D) and an open field with bare soil (plot S-E), and a sub-catchment at the temperate MDL, including a Chinese pine forest (plot T-A), larch forest (plots T-B), wetland (plots T-C), mixed broad-leaved forest (plots T-D) and open field (plots T-E) (Fig. 1). To reduce temporal uncertainty in Hg fluxes, 130-days and 96-days of flux observations were undertaken over four seasons (about one-month of continuous observations for each season, except for one-week during winter at the MDL) (Table S1). The locations of each plot is described in the Table 1 and illustrated in Fig. 1.

Semi-cylindrical quartz glass and open-bottom DFCs (4.71 L) were utilized during the sampling campaign. The area of the DFCs over the soil surface was 20 × 30 cm, with six inlet holes (1 cm diameter) (Fig. S1). Local fine grained soil was placed outside the chamber to seal any gap between the base of the chamber and the soil. At the outlet of the chamber, an orifice was connected to two exit tubes: one to a regulated suction pump and the other to a gold cartridge for trapping outlet TGM. A sub-stream of air was trapped by a pair of gold quartz cartridges at a flow rate of 0.5 L min^{-1}, which was measured using an integrating volume flow meter. All the gold cartridges were constructed with gold silk (< 0.5 mm diameter). The strands of gold silk were rolled together in a small coil and about 15 coils were used to fill a quartz cartridge with about 2 g of gold. The accuracy of all traps were evaluated (see section 2.4) and non-conforming cartridges were discarded. The chamber flushing flow turnover time (TOT) was 0.47 min and 0.94 min for the subtropical forest

and temperate forest plots, respectively. The Hg flux was calculated using the following equation:

$$F = (C_0 - C_i) \times Q/A$$

where F is the soil Hg flux (ng m^{-2} hr^{-1}); C_o and C_i are the steady state Hg concentrations (ng m^{-3}) of the outlet and inlet air streams, respectively, which were calculated by the Hg mass detected in gold cartridges and the corresponding air volume; A is the surface area enclosed by the DFC; Q is the flow rate of ambient air circulated through the DFC (10 L min^{-1} for TFP and 5 L min^{-1} for MDL).

High flow rates and short TOTs are appropriate for measuring flux from soils with high Hg concentrations or emissions, while lower flow rates and longer TOT are more appropriate for soils with low Hg concentrations or emissions. Eckley et al. (2010) suggested that the optimal flow was at the beginning of the stable $C_0 - C_i$ (ΔC) period, which was chosen as a compromise between competing criteria aimed at creating conditions inside the DFC similar to the adjacent outside air. Our previous study showed that when ΔC was relative stable, the corresponding flushing flow rate was from 5 to 10 L min^{-1} at the subtropical forest (Zhou et al., 2017a). To avoid suppression of Hg emissions due to the excessive buildup of Hg within the chamber, the flow rate of ambient air circulated through the DFC was 10 L min^{-1} at the subtropical forest. At the temperate forest, the soil Hg concentrations was about 3-4 times lower than those at the subtropical forest, so the lower flow rate of 5 L min^{-1} was used at these plots. The DFC chambers in all plots were moved every week to mitigate against changes in soil moisture due the covering of soil by the chambers. If a precipitation event occurred, the chambers were also moved to new positions during the sampling period (morning or evening) to be representative of soil conditions receiving ambient precipitation.

The pair of gold cartridges for each DFC were collected twice a day: every morning (about 8:00) and afternoon (about 17:00) representing night (17:00−8:00 of next day) and day (8:00−17:00) emissions, respectively. Twenty gold quartz cartridges were alternated during the sampling program. In addition, diurnal variations of soil-air Hg fluxes were also conducted in each season, with gold cartridges collected every half an hour. A total of four diurnal measurements were conducted over the study in each forest, with diurnal variations were measured one day per season. It has been reported that the DFC measurements can introduce bias under a given design flushing air flow rates and environmental condition (Lin et al., 2010;Zhang et al., 2002). The DFC enclosure imposes a physical constraint that can lead to accumulation in or evasion from the soil surface under measurement. Extensive experiments were conducted at our plot sites to determine the appropriate

201 experimental conditions for accurate measurements. We followed recommendations made by
202 Eckley et al. (2010) for our measurements.
203
204 **2.3. Environmental measurements**
205 At each sampling plot, soil samples were collected from the DFC footprint (0−5 cm). Soil Hg
206 and soil organic matter (SOM) concentrations were measured using a DMA-80 direct Hg analyzer
207 (Milestone Ltd., Italy) and loss on ignition (LOI) method, respectively, using methods detailed in
208 the SI. Soil percent moisture and temperature were monitored with Time Domain Reflectometry
209 (TDR) Hydra Probe II (SDI−12/RS485) and a Stevens water cable tester (USA). Solar radiation was
210 measured by a weather station (Davis Wireless Vantage VUE 06250 Weather Station, Davis
211 Instruments, Hayward, CA) located in the TFP Forest Station and Beijing Forest Ecosystem
212 Research Station, within about 500 m of each plot.
213
214 **2.4. Quality assurance and quality control (QA/QC)**
215 All cartridges were transported to a laboratory at the TFP Forest Station for Hg determination
216 using a cold vapor atomic fluorescence spectroscopy (CVAFS) detector (Brooks Rand III). The limit
217 of detection, based on three times the standard deviation of replicate measurements of the blank was
218 1 pg. Based on the sampled air volume, the detection limits were < 0.10 ng m^{-3}. A calibration curve
219 was developed using Hg saturated air and the calibration curve was required to have a correlation
220 coefficient greater than 0.99 before the samples analysis could proceed. Before and after the
221 measurement of the sampling cartridges in each day, standard Hg saturated air was injected to test
222 the accuracy of the Hg analyzer. If the deviation of the measured Hg mass was higher than 5%, new
223 calibration curve would be developed.
224 A controlled volume of saturated Hg air at a known temperature was injected to measure Hg
225 recovery from the gold cartridges before and after the campaigns in each season. The recoveries of
226 gold cartridges before and after the operation ranged from 98.8 to 103.2% and 96.3 to 102.5%
227 (n=155, average=98.9%), respectively. The collection efficiency of Hg vapor by the gold cartridges
228 was determined by connecting two cartridges in sequence and sampling the ambient air over 24 h
229 in the laboratory. For all cartridges, less than 1% Hg was detected on the second cartridges compared
230 to the first cartridge, indicating that more than > 99% of TGM was absorbed by the gold cartridges

during the field operation. For comparison, Hg fluxes were measured by two chambers side by side simultaneously. Blanks of the soil TGM flux sampling systems were measured by placing the DFC on a quartz glass surface in the five plots. The sampling time for blank measurements was same as soil-air TGM flux measurements, which were collected at 8:00 and 17:00, representing night (17:00−8:00 of next day) and day (8:00−17:00) emissions, respectively. The averaged blank was 0.13 ± 0.21 ng m^{-2} h^{-1} (n=10), which was subtracted from the soil-air TGM flux for each season.

2.5. Statistical analysis

Structural equation modeling (SEM) were performed on the collected Hg flux data using Amos software. SEM, developed from a fully conceptual model using $\chi 2$ tests with maximum likelihood estimation, was conducted to infer the interplay of temperature, solar radiation, soil moisture, and air TGM concentrations on measurements of soil-air TGM exchange fluxes. Seasonal and annual fluxes were compared among the ten plots. Separate two-way ANOVAs were used to determine if differences in Hg fluxes existed among the seasons and sites. All differences in mean values were significant at the p=0.05 level and all means are reported with ± one standard deviation from the mean. The correlations between environmental parameters and fluxes were analyzed by Pearson's Correlation Tests using SPSS software (SPSS Inc. 16.0) and correlation coefficient and p values are presented and significantly correlated at the level of 0.05.

3. Results and discussion

3.1. Landscape- and forest species-dependence of soil-air Hg fluxes at the forest catchment scale

The soil TGM flux measurements for the five plots were calculated for the day and night and reported as mean daily fluxes with standard deviations (SD) at the subtropical (Fig. 2a) and temperate forests (Fig. 2b). Over the course of the campaigns, net TGM emission was observed at the open field (24 ± 33 ng m^{-2} hr^{-1}), coniferous forest (upper elevation 2.8 ± 3.9 ng m^{-2} hr^{-1}, mid elevation 3.5 ± 4.2 ng m^{-2} hr^{-1}) and the broad-leaved forest (0.18 ± 4.3 ng m^{-2} hr^{-1}), while net deposition was evident at the wetland (−0.80 ± 5.1 ng m^{-2} hr^{-1}), respectively, at the subtropical forest. At the temperate forest, net TGM emission was observed at the wetland (3.81 ± 0.52 ng m^{-2} hr^{-1}), open field (1.82 ± 0.79 ng m^{-2} hr^{-1}), mixed broad-leaved forest (0.68 ± 1.01 ng m^{-2} hr^{-1}),

larch forest (0.32 ± 0.96 ng m^{-2} hr^{-1}), while net deposition was evident at the Chinese pine forest (−0.04 ± 0.81 ng m^{-2} h^{-1}), respectively. The fluxes at the temperate forest were 10-times lower than values at the subtropical forest due to different environmental factors, such as lower temperature, solar radiation and soil Hg concentrations (see section 3.3).

These patterns suggest that soil-air Hg fluxes at catchment scale vary by soil properties (e.g., soil Hg concentration, moisture, SOM) and forest species composition. High variability, as evidenced by high SD and coefficient of variation (SD/mean, range of 14−2374%), was evident in daily Hg fluxes largely driven by meteorological variation. The fluxes at the subtropical forest plots of this study were much lower than those reported for other subtropical evergreen forests in China such as Mt. Gongga (0.5–9.3 ng m^{-2} hr^{-1}) (Fu et al., 2008), Mt. Jinyun (14.2 ng m^{-2} hr^{-1}) (Ma et al., 2013) and Mt. Simian (11.23 ng m^{-2} hr^{-1}) (Ma et al., 2018), all of which were generally conducted during sunny days. Our flux measurements at temperate forest were slightly lower or comparable to those in North American deciduous forests, ranging from −0.73 to 2.7 ng m^{-2} hr^{-1} (Choi and Holsen, 2009b;Hartman et al., 2009;Carpi et al., 2014;Ma et al., 2018). These results demonstrated that measurements over several days may exhibit considerable temporal variability and long-term study should be undertaken to reduce the uncertainty in temporal patterns of soil Hg emissions.

The mean TGM fluxes in the open fields were about 10 and 6 times higher than those under the forest canopy at the subtropical and temperate forests, respectively ($p < 0.001$). Our results are consistent with Ma et al. (2013) and Xin and Gustin (2007), showing large Hg evasion following forest conversion to bare soils due to direct exposure to sunlight, as fluxes were enhanced by increases in solar radiation and temperature. Due to frequent heavy rains at the subtropical forest catchment, a large amount of surface runoff impacted the wetland (plot S-C). Elevated runoff may have decreased Hg (96 ± 43 ng g^{-1}) and SOM in surface soils due to erosion (Table 1). This site had the lowest TGM fluxes of the plots studied at the subtropical forest (overall net sink). In addition, soils in the wetland plot were mostly saturated throughout the year, limiting Hg fluxes and likely contributing to the sink behavior. In contrast, the mean annual rainfall was 40% lower at the temperate forest and the wetland was located at relatively lower terrain. Litter from surrounding higher terrain forest accumulated in the low lying wetland. The cool and dry climate also contributed to high organic matter and low bulk density (Fang et al., 2007). Higher SOM likely facilitated

291 binding of trace metals, leading to high soil Hg concentrations (117 ng g^{-1}) at the temperate wetland.
292 These conditions were conducive to biological activity, promoting the mineralization of SOM and
293 the release of volatile Hg(0) from soil (Choi and Holsen, 2009b;Osterwalder et al., 2019). The
294 wetland had the highest TGM fluxes of the plots studied at the temperate forest (overall net source).
295 Previous studies have suggested that soil water is able to mobilize Hg from binding sites on soil
296 (Gustin, 2003;Kocman and Horvat, 2010) and high soil water decreases soil redox potential (Zarate-
297 Valdez et al., 2006), both of which can facilitate the conversion of Hg(II) to Hg(0). Additionally, the
298 climate is relatively dry in north China, especially in spring. The high solar radiation and relatively
299 high air temperature not only enhance the reduction of Hg(II) to Hg(0), but also increase water
300 evaporation compared to other study sites. Enhanced water evaporation at higher temperature,
301 facilitates Hg emissions from soils (Gustin and Stamenkovic, 2005;Lin et al., 2010). Additionally,
302 given that Hg conversion to Hg(0) in soil profiles occurs mainly via biotic processes, maximum
303 aerobic microbial activity has been delineated at soil water content equivalent to 60% of a soil's
304 water holding capacity (Breuer et al., 2002;Kiese and Butterbach-Bahl, 2002). Appropriate soil
305 moisture in the wetland would likely enhance the microbial reduction of Hg(II) to Hg(0). Therefore,
306 the highest Hg flux was observed in the temperate wetland, especially in spring. The main reasons
307 for the significant differences between the soil Hg fluxes at the two wetland sites is likely that the
308 saturated soil at the subtropical forest inhibited Hg(0) evasion (Gustin and Stamenkovic, 2005) (see
309 section 3.3).
310 At the subtropical forest, litterfall in the broad-leaved (camphor) plot (plot S-D) was twice as
311 high as that of the coniferous (pine) plot (plots S-A and S-B) (Zhou et al., 2018), likely resulting in
312 greater shielding of sunlight to the surface soil and limiting soil Hg evasion. Increases in light
313 transmission through the canopy increase both solar radiation and soil temperature, which can
314 enhance photochemical reduction of Hg(II) at the soil surface and Hg(0) evasion. In the mid-slope
315 of the pine stand (plot S-B), soil Hg concentration was elevated compared to the upslope plot (Table
316 1), with corresponding with higher soil Hg fluxes. At the temperate forest, the lowest Hg flux and
317 overall deposition was observed at the evergreen forest of Chinese pine, where the canopy cover
318 likely limited Hg flux by decreasing solar radiation to soil and warming. Similar at the subtropical
319 forest, the needle biomass in the larch plot was about 2.5 times greater as that in the mixed broad-
320 leaved plot (plot T-D) at the temperate forest, resulting in shielding the sunlight to the surface soil

and limiting soil Hg evasion at larch plot.

The forest canopy not only influences the soil Hg concentration by mediating atmospheric Hg deposition (Zhou et al., 2018;Zhou et al., 2017a), but also alters soil physio-chemical properties (e.g. SOM, pH, porosity) (Mo et al., 2011) and microbial communities (Nagati et al., 2020), which affect soil-air exchange. For example, the annual litterfall Hg deposition flux at the broad-leaved plot (91 μg m^{-2} yr^{-1}) at the subtropical forest was approximately two times greater than the coniferous plot (41 μg m^{-2} yr^{-1}) (Zhou et al., 2018). Conversely, the SOM and soil Hg concentrations in the broad-leaved forest were lower than the coniferous forest. Moreover, litter decomposition rate was lower, but the Hg mass accumulation in the litter was much higher in the coniferous forest compared to the broad-leaved forest due to higher throughfall Hg deposition at the coniferous plot (Zhou et al., 2018), which resulted in a seemingly inconsistent pattern between litterfall mass and SOM, as well as litterfall Hg deposition and soil Hg concentrations. At the temperate forest, the higher litterfall Hg deposition and lower litter decomposition in the larch plot compared to the broad-leaved plot (Zhou et al., 2017a), resulted in significant higher SOM and soil Hg concentrations (Table 1). Tree species can change the physicochemical properties of soil (e.g. SOM, soil Hg concentrations) and influence soil-air exchange. These biological factors likely contribute to the much lower TGM evasion in the broad-leaved plot than the coniferous plot at the subtropical forest, but much higher TGM evasion in the broad-leaved plot than the deciduous needle (larch) plot at the temperate forest (Fig. 2).

Most studies measure soil TGM fluxes at only one location or at a single forest stand to characterize the whole ecosystem. Our observations clearly show that soil-air Hg fluxes vary substantially across different plots (Fig. 2), indicating that forest type/cover and landscape position significantly affect the TGM fluxes and therefore the spatial variability in soil Hg fluxes among different sub-plots must be considered. Based on the areal distribution of each plot type in the study sub-catchments of the subtropical forest (coniferous upland and mid-slope, broad-leaved, wetland, open) (4.6 ha) and the temperate forest (Chinese pine, larch, wetland, mixed broad-leaved and open) (5.0 ha) (Table S1), the area-weighted TGM flux was 3.2 and 0.32 ng m^{-2} hr^{-1} for the entire subtropical and temperate catchments, respectively. The area-weighted TGM fluxes were 14% higher than plot S-A and 16% lower than plot S-B of the Masson pine stand at the subtropical forest, and were 907% higher than Chinese pine plot and 53% lower than mixed broad-leaved plot at the temperate forest, respectively. The observations at several plots with diverse forest cover in

this study should reduce the overall uncertainty associated with soil-air fluxes of TGM in the overall forest catchment.

3.2. Seasonal variations of soil-air Hg fluxes at the forest catchment scale

Soil TGM fluxes not only exhibited clear seasonal variations at all the plots, but also were responsive to phenological and meteorological patterns. At the subtropical forest, soil Hg fluxes were generally highest in the summer (Fig. 2a), which showed net emissions at all the five plots, followed by spring and autumn, with the lowest values during winter, which exhibited net deposition at all plots with the exception of plot S-B. The observed seasonal variation was dependent on sunlight (Fig. 3), because solar radiation drives photochemical reduction of Hg(II) (note the correlation between the TGM fluxes and solar radiation, Fig. S2). Additionally, greater solar radiation increases temperature, which promotes the production of soil Hg gas by biological and abiotic processes. At the temperate forest, the Hg fluxes were the highest in the deciduous forest plot (wetland, mixed broad-leaved forest and larch forest) in spring before leaf-out when solar radiation could directly reach the forest floor (Fig. S3). In the open field and evergreen forest (Chinese pine forest) plots, the Hg fluxes were highest in summer with the highest solar radiation and temperature (Fig. 4 and Fig. S3). The lowest Hg fluxes were measured in the winter at all plots when the soil was covered with snow, with net Hg emission observed at the open field and net deposition observed at the other four sites (Fig. 2b).

We also observed strong variation in TGM evasion under different weather conditions. Rain events decreased TGM fluxes at all plots in both forests (Fig. S4), as the rainwater decreased soil pore space leading to decreases in evasion from soil. Furthermore, the solar radiation and temperature during rainy days was much lower than those for sunny days for a given season (Fig. 3 and Fig. 4). Manca et al. (2013) studied snow-air Hg exchange at Ny-Ålesund, showing on average a small net deposition -0.24 ng m^{-2} hr^{-1}. Likewise, overall deposition between -0.6 and -23.8 ng m^{-2} hr^{-1} were observed at snow-covered agricultural areas at Northeastern China (Wang et al., 2013;Zhang et al., 2013). However, some studies of snowpack have shown net Hg deposition at nighttime and net emissions during daytime due to high solar radiation (Maxwell et al., 2013;Spolaor et al., 2019). Empirical models suggest that most of the Hg(0) deposited to snow was re-emitted back to the atmosphere (Durnford and Dastoor, 2011). During the campaigns in winter,

381 the solar radiation was relatively lower, which may be why net deposition occurred (Fig. 4).
382 Additionally, refrozen ice/snow layers are characterized by elevated Hg concentrations and the
383 deposited Hg from atmosphere could be potentially released to meltwater (Zhang et al., 2012;Perez-
384 Rodriguez et al., 2019), which is consistent with our results that atmospheric Hg deposition could
385 release to meltwater during snow melt. Our observations through the annual climatic cycle reduce
386 uncertainty and bias of temporal patterns of soil-air Hg fluxes. Moreover, multi-plot observations
387 reduce the uncertainty and bias associated with spatial variation. Together these more detailed
388 measurements improved estimates of overall ecosystem soil Hg evasion, and confirm our hypothesis.
389
390 **3.3. Correlations between environmental factors and fluxes**
391 To investigate the correlation between soil-atmosphere fluxes and environmental factors, data
392 over the four seasons were used. These data offer a long continuous time series for the five
393 measurement plots in each forest (Fig. 3 and 4). According to a global database, atmospheric fluxes
394 at Hg-enriched sites are positively correlated with substrate Hg concentrations, but this relationship
395 is not observed at sites with lower background concentrations of soil Hg (Agnan et al., 2016). Our
396 soil Hg fluxes were strongly correlated with soil Hg concentrations at vegetated sites (forests and
397 wetland) at the subtropical forest (Fig. S5), but not at the temperate forest.
398 Photo-reduction is a major driver of TGM evasion from the Earth's surface (Howard and
399 Edwards, 2018;Kuss et al., 2018;Gao et al., 2020). This process is due to photochemically mediated
400 reduction that converts soil water Hg(II) to volatile Hg(0) and enhances the Hg(0) pool in soil pores
401 (Xin and Gustin, 2007;Choi and Holsen, 2009a). Therefore, the elevated soil pore Hg(0)
402 concentrations increased the potential for TGM diffusion from soil to the atmosphere, which drives
403 an increase of Hg emissions from soil. At all the study sites no matter the daily average fluxes (Fig.
404 3 and 4), daytime fluxes (Fig. S2 and S3) were all significantly correlated with solar radiation, and
405 the solar radiation also increased daytime fluxes compare to nighttime values (Fig. S6). In the
406 evergreen plots of the subtropical (plots S-A, S-B, S-D) and temperate (plot T-A) forests, Hg fluxes
407 were the most highly dependent on soil temperature compared to the solar radiation during the four
408 seasons, likely due to evergreen canopy limiting solar radiation to the forest floor. With the
409 consistent shade of the coniferous forest canopy, the Hg flux was highly dependent on soil surface
410 temperature rather than solar radiation to the forest floor.

411 To consider synergistic effects from multiple factors, SEM was applied to infer the soil-air
412 TGM exchange processes (Fig. 5). It is clear that temperature was a more dominant factor driving
413 air-soil TGM exchange flux over the four seasons in the subtropical forest plots, while solar
414 radiation was a more dominant factor at the temperate forest due to direct exposure of the forest
415 floor to solar radiation the leaf-off seasons. At the open fields of both forests, temperature and solar
416 radiation had a synergistic effect on soil Hg fluxes. A recent study of soil-air TGM fluxes at
417 subtropical evergreen broadleaf forest in South China also suggested that temperature is the most
418 important driver of air-soil TGM exchange (Yuan et al., 2019b). Therefore, we may infer that under
419 the shade of the forest canopy, temperature is the dominant factor causing variation in TGM evasion
420 from forest soil.
421 Mercury fluxes in wetlands in both forests (plots S-C and T-C) were less strongly correlated
422 with soil temperature compared to the other plots in both forests (Fig. S7 and S8). Generally,
423 temperature is an important factor that promotes TGM evasion after its formation from Hg(II) more
424 by biotic than abiotic processes in soils (Pannu et al., 2014). The Hg(0) in soil pore gas mainly
425 results from biotic production. For example, soil sterilization can decrease Hg converted to Hg(0)
426 by ~50% ; additionally, 1% of the soil Hg is converted to Hg(0) via abiotic processes, compared to
427 6.8% by biotic processes at 283 K, and the fraction of Hg reduction by biotic processes increases
428 with temperature increases (Pannu et al., 2014). At the subtropical forest, the wetland soil was
429 largely saturated. This condition likely limited soil pore release of TGM to the atmosphere, resulting
430 in a weaker correlation between soil temperature and Hg fluxes. Furthermore, the Hg exchange
431 fluxes were more dependent on solar radiation and less dependent on temperature during the leaf-
432 off period at the temperate deciduous plots; therefore, the Hg fluxes were more solar radiation-
433 driven in the deciduous forests, especially in the wetland (Fig. S3 and S7).
434 During the campaign, significant negative correlations were evident between soil moisture and
435 soil-air fluxes of TGM at the five plots at the subtropical forest (r^2= 0.03−0.39, $p < 0.05$ for all, Fig.
436 S9), but there was no significant correlations with soil moisture for the temperate forest (Fig. S10).
437 Generally there is an optimum soil moisture condition that maximizes soil TGM flux (Gustin and
438 Stamenkovic, 2005;Lin et al., 2010;Obrist et al., 2014;Osterwalder et al., 2018;Johnson et al., 2003),
439 which ranges from 60% to 80% of the water holding capacity of a soil (Pannu et al., 2014). A
440 laboratory experiment using undisturbed soil collected from the our subtropical study area showed

that increasing soil moisture from 2% to 20% increased the TGM flux 80% at 24 °C (Wang et al., 2014). A second field experiment was conducted to study the effects of higher soil moisture on TGM flux at the subtropical forest, showing that increasing soil moisture gradually decreased the soil Hg emissions over the range of 31−39% (Zhou et al., 2017b). Combining the results of these experiments, the soil Hg fluxes at the subtropical forest catchment appear to increase from low values of soil moisture reaching an optimum in the range of 20-30% and then decreasing with increasing soil moisture above these values. In the current study, we observed following an extended dry period with an extended wet period enhanced the Hg fluxes in both forests; however, individual rainfall events did not enhance or decrease the Hg fluxes due to short-term increases in soil moisture and lower solar radiation associated with those events (Fig. 3 and 4). Additionally, Lin et al. (2010) observed the synergistic effects (20–30 % of additional flux enhancement) between air temperature (15 and 30 °C) and soil moisture (2.5 and 27.5 %). Perennially humid weather results in relatively high soil moisture at the subtropical forest (largely > 25% during the campaigns). Considering the relatively high bulk density and low porosity of soil at the subtropical forest (Sørbotten, 2011), soil moisture likely exceeded the optimum range for TGM evasion during the campaigns resulting in significantly negative correlations (Fig. S9). In contrast, lower bulk density and higher soil porosity would result in higher optimum range of soil moisture at the temperate forest. Moreover, the temperate forest had a large range of soil moisture (2 to 60%) in the five plots which combined with the synergistic effects of soil moisture with temperature (Lin et al., 2010), resulted in a condition where moisture was not a main driver of TGM evasion.

Soil-air Hg fluxes also showed significant negative correlations with atmospheric TGM concentrations at the ten plots at both forests ($r^2 = 0.023−0.26$, $p < 0.05$, Fig. 6 and 7), which had a greater effect than soil moisture at both forests, except for plots T-C, S-A and S-E (Fig. 5). According to the two-resistance exchange interface model, the exchange fluxes of Hg are controlled by the gradient of TGM concentrations at both interfaces (Zhang et al., 2002). As a result elevated atmospheric TGM concentrations should decrease the diffusion of soil pore TGM to the atmosphere. In a companion study, the soil pore TGM concentrations were measured at all the plots at the subtropical and temperate forests, except the wetlands (Zhou et al., in review). These results showed that gradient of TGM concentrations between the surface air and pore air at 3 cm were significantly correlated with the soil-air TGM fluxes at all the plots (Fig. S11 and S12). These results are

consistent with an experiment conducted at this subtropical forest, where artificially increasing ambient-air TGM concentrations significantly inhibited soil Hg volatilization (Zhou et al., 2017b). SEM inferred that that air TGM concentrations was the second important driver influencing the soil-air TGM exchange in Masson pine (Plot S-B), evergreen broad-leaved and wetland plots at subtropical forest (Fig. 5).

Xin and Gustin (2007) and Gustin et al. (2006) defined an associated concept of the compensation point for soils, which is the atmospheric Hg concentration at which the net Hg flux between the soil and the atmosphere was zero. If the atmospheric TGM concentration is above compensation point, atmospheric deposition occurs; if the concentration is below the compensation point soil emission occurs. A strong linear relationships are shown in Figs. 5 and 6 ($p < 0.01$), resulting in compensation points of 2.47, 2.97, 6.00, 3.33 and 3.50 ng m^{-3} for Chinese pine, larch, wetland, mixed broad-leaved forests and open field at the temperate forest with area-weighted compensation point of 3.42 ng m^{-3}. The compensation points were much higher at the subtropical forest, with values of 6.50, 7.71, 3.92, 3.83 and 12.91 ng m^{-3} for Masson pine upland and mid-slope, wetland, broad-leaved and open field at the subtropical forest with area-weighted compensation point of 6.82 ng m^{-3}. Another study of subtropical coniferous forest showed similar compensation point (7.75 ng m^{-3}) as those in the Masson pine forests of our study (Luo, 2015).

Diurnal variation in soil-air TGM fluxes were measured in plot S-A at the subtropical forest (Fig. 8) and in plot T-D at the temperate forest (Fig. 9). Soil TGM fluxes were well correlated with soil and air temperature ($p < 0.01$ for all) and were highly dependent on solar radiation in spring, summer and autumn ($p < 0.01$ for all) but not in winter ($p > 0.05$), which are similar to seasonal patterns from other studies (Howard and Edwards, 2018;Osterwalder et al., 2018;Johnson et al., 2003). Solar radiation has been shown to promote photochemical reduction of soil-bound Hg and enrich Hg(0) in soil pore gas. This reaction is kinetically enhanced at higher temperatures (Eckley et al., 2015;Lin et al., 2010;Zhang et al., 2001). Compared to the other three seasons, the relatively low soil temperature (5.95 °C at the subtropical forest and –5.66 °C at the temperate forest) may have limited the relationship between soil TGM flux and solar radiation during the winter season.

4. Conclusions and study implications

Prior to undertaking these measurements of Hg air-surface exchange flux, no direct

measurement of Hg exchange flux were available for background landscapes in North China. Our detailed direct observations have important implications for the role of forests in global and regional Hg cycles. Through multi-plot measurements over 130 and 96 days at the subtropical and temperate forests in China, we were able to reduce the uncertainty of soil-atmosphere TGM fluxes at the catchment scale and improve understanding of how landscape attributes contribute to variability in soil Hg evasion. It is inferred that forest soils acts as net TGM sources to the atmosphere. Strong correlations were evident between the soil Hg flux and environmental variables in some plots, such as solar radiation, temperature, soil moisture and air TGM concentrations.

The compensation points were determined for background forest soils from full-scale field data showing area-weighted values of 6.82 and 3.42 ng m^{-3} for the entire subtropical and temperate catchments, respectively. The values of compensation indicate that the atmospheric TGM concentration can play a critical role in limiting TGM fluxes between forest floor and atmosphere. Future studies need to focus on forest soils as an important increasing source of Hg to the atmosphere, because of recent declines in anthropogenic Hg emissions and TGM concentrations (Liu et al., 2019). Moreover TGM re-emissions are partially derived from legacy Hg stored in surface soils. A recent study using models simulating the dynamics of the subtropical forest landscape under climate change, harvesting, and land-use disturbances in southern China showed that coniferous forest area increased approximately 3.7 times compared to broad-leaved forest area (Wu et al., 2019). In the temperate forest, climatic changes in the northern China are expected to cause coniferous stands to transition to deciduous forests over the next hundred years (Ma et al., 2014). Climate change and land-use disturbance may increase the compensation points in both temperate and subtropical forests, therefore, increasing emissions of legacy Hg from terrestrial soils to the atmosphere. Some studies have emphasized that climate and land use change will potentially enhance deposition of Hg to forested landscapes (Haynes et al., 2017;Richardson and Friedland, 2015;Li et al., 2020); however, our study suggests that legacy Hg in forest soils could be emitted back to atmosphere, offsetting enhanced atmospheric Hg deposition. Better understanding of the response of Hg emissions from forest soils to climate and land use change is an important topic for future research.

Data availability. The data will be available upon request to the corresponding author.

Author contributions. ZW and XZ conceived the experiment; JZ conducted the measurements; JZ wrote the paper with inputs from CTD, CL and ZW. All authors reviewed the manuscript.

Competing interests. The authors declare that they have no conflict of interest.

Acknowledgements. This work was funded by the Second Tibetan Plateau Scientific Expedition and Research Program (STEP, Grant No. 2019QZKK0307), the Natural Science Foundation of China (No.42077345 and No. 42077381)，the National 973 Program of China (2013CB430002) and the National Key Research and Development Program of China (2017YFC0210106). The authors would like to thank Mingquan Zou and Beijing Forest Ecosystem Research Station, Chinese Academy of Sciences, for the help in our sampling and providing the meteorological data.

References:

Agnan, Y., Le, D. T., Moore, C., Edwards, G., and Obrist, D.: New constraints on terrestrial surface-atmosphere fluxes of gaseous elemental mercury using a global database, Environmental Science & Technology, 50, 507−524, 10.1021/acs.est.5b04013, 2016.

Angot, H., Dastoor, A., De Simone, F., Gardfeldt, K., Gencarelli, C. N., Hedgecock, I. M., Langer, S., Magand, O., Mastromonaco, M. N., Nordstrom, C., Pfaffhuber, K. A., Pirrone, N., Ryjkov, A., Selin, N. E., Skov, H., Song, S., Sprovieri, F., Steffen, A., Toyota, K., Travnikov, O., Yang, X., and Dommergue, A.: Chemical cycling and deposition of atmospheric mercury in polar regions: review of recent measurements and comparison with models, Atmospheric Chemistry and Physics, 16, 10735-10763, 10.5194/acp-16-10735-2016, 2016.

Breuer, L., Kiese, R., and Butterbachbahl, K.: Temperature and moisture effects on nitrification rates in tropical rain-forest soils, Soil Science Society of America Journal, 66, 399-402, 2002.

Carpi, A., Fostier, A. H., Orta, O. R., dos Santos, J. C., and Gittings, M.: Gaseous mercury emissions from soil following forest loss and land use changes: Field experiments in the United States and Brazil, Atmospheric Environment, 96, 423-429, 10.1016/j.atmosenv.2014.08.004, 2014.

Chen, Y., Yin, Y., Shi, J., Liu, G., Hu, L., Liu, J., Cai, Y., and Jiang, G.: Analytical methods, formation, and dissolution of cinnabar and its impact on environmental cycle of mercury, Critical Reviews in Environmental Science and Technology, 47, 2415-2447, 10.1080/10643389.2018.1429764, 2017.

Cheng, Z., Tang, Y., Li, E., Wu, Q., Wang, L., Liu, K., Wang, S., Huang, Y., and Duan, L.: Mercury accumulation in soil from atmospheric deposition in temperate steppe of Inner Mongolia, China, Environmental Pollution, 258, 10.1016/j.envpol.2019.113692, 2020.

Choi, H.-D., and Holsen, T. M.: Gaseous mercury emissions from unsterilized and sterilized soils: The effect of temperature and UV radiation, Environmental Pollution, 157, 1673-1678, 10.1016/j.envpol.2008.12.014, 2009a.

Choi, H. D., and Holsen, T. M.: Gaseous mercury fluxes from the forest floor of the Adirondacks,

569 Environmental Pollution, 157, 592-600, 2009b.
570 Du, B., Zhou, J., Zhou, L., Fan, X., and Zhou, J.: Mercury distribution in the foliage and soil profiles of
571 a subtropical forest: Process for mercury retention in soils, Journal of Geochemical Exploration, 205,
572 10.1016/j.gexplo.2019.106337, 2019.
573 Durnford, D., and Dastoor, A.: The behavior of mercury in the cryosphere: A review of what we know
574 from observations, Journal of Geophysical Research: Atmospheres, 116, 10.1029/2010jd014809,
575 2011.
576 Eckley, C. S., Gustin, M., Lin, C. J., Li, X., and Miller, M. B.: The influence of dynamic chamber design
577 and operating parameters on calculated surface-to-air mercury fluxes, Atmospheric Environment, 44,
578 194-203, 10.1016/j.atmosenv.2009.10.013, 2010.
579 Eckley, C. S., Blanchard, P., Mclennan, D., Mintz, R., and Sekela, M.: Soil–air mercury flux near a large
580 industrial emission source before and after closure (Flin Flon, Manitoba, Canada), Environmental
581 Science & Technology, 49, 9750-9757, 2015.
582 Fang, J., Liu, G., Zhu, B., Wang, X., and Liu, S.: Carbon budgets of three temperate forest ecosystems
583 in Dongling Mt., Beijing, China, Science in China Series D-Earth Sciences, 50, 92-101,
584 10.1007/s11430-007-2031-3, 2007.
585 FAO: UNESCO soil map of the world, revised legend, in, World Res. Rep., 138, 1988.
586 Fraser, A., Dastoor, A., and Ryjkov, A.: How important is biomass burning in Canada to mercury
587 contamination?, Atmospheric Chemistry and Physics, 18, 7263-7286, 10.5194/acp-18-7263-2018,
588 2018.
589 Fu, X., Feng, X., and Wang, S.: Exchange fluxes of Hg between surfaces and atmosphere in the eastern
590 flank of Mount Gongga, Sichuan province, southwestern China, Journal of Geophysical Research-
591 Atmospheres, 113, 253-270, 2008.
592 Gao, Y., Wang, Z., Zhang, X., and Wang, C.: Observation and estimation of mercury exchange fluxes
593 from soil under different crop cultivars and planting densities in North China Plain, Environmental
594 pollution, 259, 113833, 10.1016/j.envpol.2019.113833, 2020.
595 Gustin, M. S.: Are mercury emissions from geologic sources significant? A status report, Science of the
596 Total Environment, 304, 153, 2003.
597 Gustin, M. S., and Stamenkovic, J.: Effect of watering and soil moisture on mercury emissions from soils,
598 Biogeochemistry, 76, 215-232, 2005.
599 Gustin, M. S., Engle, M., Ericksen, J., Lyman, S., Stamenkovic, J., and Xin, M.: Mercury exchange
600 between the atmosphere and low mercury containing substrates, Applied Geochemistry, 21, 1913-
601 1923, 2006.
602 Hararuk, O., Obrist, D., and Luo, Y.: Modelling the sensitivity of soil mercury storage to climate-induced
603 changes in soil carbon pools, Biogeosciences, 10, 2393-2407, 2013.
604 Hartman, J. S., Weisberg, P. J., Pillai, R., Ericksen, J. A., Kuiken, T., Lindberg, S. E., Zhang, H., Rytuba,
605 J. J., and Gustin, M. S.: Application of a rule-based model to estimate mercury exchange for three
606 background biomes in the continental United States, Environmental Science & Technology, 43, 4989-
607 4994, 10.1021/es900075q, 2009.
608 Haynes, K. M., Kane, E. S., Potvin, L., Lilleskov, E. A., Kolka, R. K., and Mitchell, C. P. J.: Gaseous
609 mercury fluxes in peatlands and the potential influence of climate change, Atmospheric Environment,
610 154, 247-259, https://doi.org/10.1016/j.atmosenv.2017.01.049, 2017.
611 Hou, H. Y.: Vegetation Map of P.R. China(1:4, 000, 000), Beijing, 1982.
612 Howard, D., and Edwards, G. C.: Mercury fluxes over an Australian alpine grassland and observation of

nocturnal atmospheric mercury depletion events, Atmospheric Chemistry and Physics, 18, 129-142, 10.5194/acp-18-129-2018, 2018.
Johnson, D. W., Benesch, J. A., Gustin, M. S., Schorran, D. S., Lindberg, S. E., and Coleman, J. S.: Experimental evidence against diffusion control of Hg evasion from soils, Science of the Total Environment, 304, 175, 2003.
Kamp, J., Skov, H., Jensen, B., and Sorensen, L. L.: Fluxes of gaseous elemental mercury (GEM) in the High Arctic during atmospheric mercury depletion events (AMDEs), Atmospheric Chemistry and Physics, 18, 6923-6938, 10.5194/acp-18-6923-2018, 2018.
Kiese, R., and Butterbach-Bahl, K.: N2O and CO2 emissions from three different tropical forest sites in the wet tropics of Queensland, Australia, Soil Biology & Biochemistry, 34, 975-987, 2002.
Kocman, D., and Horvat, M.: A laboratory based experimental study of mercury emission from contaminated soils in the River Idrijca catchment, Atmospheric Chemistry and Physics, 10, 1417-1426, 2010.
Kumari, A., Kumar, B., Manzoor, S., and Kulshrestha, U.: Status of Atmospheric Mercury Research in South Asia: A Review, Aerosol and Air Quality Research, 15, 1092-1109, 10.4209/aaqr.2014.05.0098, 2015.
Kuss, J., Krueger, S., Ruickoldt, J., and Wlost, K.-P.: High-resolution measurements of elemental mercury in surface water for an improved quantitative understanding of the Baltic Sea as a source of atmospheric mercury, Atmospheric Chemistry and Physics, 18, 4361-4376, 10.5194/acp-18-4361-2018, 2018.
Li, F., Ma, C., and Zhang, P.: Mercury Deposition, Climate Change and Anthropogenic Activities: A Review, Frontiers in Earth Science, 8, 10.3389/feart.2020.00316, 2020.
Lin, C. J., Gustin, M. S., Singhasuk, P., Eckley, C., and Miller, M.: Empirical models for estimating mercury flux from soils, Environmental Science & Technology, 44, 8522-8528, 2010.
Lin, H., Tong, Y., Yin, X., Zhang, Q., Zhang, H., Zhang, H., Chen, L., Kang, S., Zhang, W., Schauer, J., de Foy, B., Bu, X., and Wang, X.: First measurement of atmospheric mercury species in Qomolangma Natural Nature Preserve, Tibetan Plateau, and evidence of transboundary pollutant invasion, Atmospheric Chemistry and Physics, 19, 1373-1391, 10.5194/acp-19-1373-2019, 2019.
Liu, K., Wu, Q., Wang, L., Wang, S., Liu, T., Ding, D., Tang, Y., Li, G., Tian, H., Duan, L., Wang, X., Fu, X., Feng, X., and Hao, J.: Measure-specific effectiveness of air pollution control on China's atmospheric mercury concentration and deposition during 2013-2017, Environmental Science & Technology, 53, 8938-8946, 10.1021/acs.est.9b02428, 2019.
Luo, Y.: Mercury input, output and transport in forest ecosystems in southern China, Doctor’s dissertation, Tsinghua University, Beijing, China, , pp. 1–112 pp., 2015.
Ly Sy Phu, N., Zhang, L., Lin, D.-W., Lin, N.-H., and Sheu, G.-R.: Eight-year dry deposition of atmospheric mercury to a tropical high mountain background site downwind of the East Asian continent, Environmental Pollution, 255, 10.1016/j.envpol.2019.113128, 2019.
Ma, J., Hu, Y., Bu, R., Chang, Y., Deng, H., and Qin, Q.: Predicting Impacts of Climate Change on the Aboveground Carbon Sequestration Rate of a Temperate Forest in Northeastern China, Plos One, 9, 10.1371/journal.pone.0096157, 2014.
Ma, M., Wang, D., Sun, R., Shen, Y., and Huang, L.: Gaseous mercury emissions from subtropical forested and open field soils in a national nature reserve, southwest China, Atmospheric Environment, 64, 116-123, 2013.
Ma, M., Sun, T., Du, H., and Wang, D.: A Two-Year Study on Mercury Fluxes from the Soil under

Different Vegetation Cover in a Subtropical Region, South China, Atmosphere, 9, 10.3390/atmos9010030, 2018.
Manca, G., Ammoscato, I., Esposito, G., Ianniello, A., Nardino, M., and Sprovieri, F.: Dynamics of snow-air mercury exchange at Ny Ålesund during springtime 2011, E3S Web of Conferences, 1, 03010, 2013.
Maxwell, J. A., Holsen, T. M., and Mondal, S.: Gaseous elemental mercury (GEM) emissions from snow surfaces in northern New York, Plos One, 8, e69342, 2013.
Mo, F., Li, X., He, S., and Wang, X.: Evaluation of soil and water conservation capacity of different forest types in Dongling Mountain, Shengtai Xuebao/Acta Ecologica Sinica, 31, 5009-5016, 2011.
Nagati, M., Roy, M., DesRochers, A., Bergeron, Y., and Gardes, M.: Importance of soil, stand, and mycorrhizal fungi inabiesbalsameaestablishment in the boreal forest, Forests, 11, 10.3390/f11080815, 2020.
O'Connor, D., Hou, D., Ok, Y. S., Mulder, J., Duan, L., Wu, Q., Wang, S., Tack, F. M. G., and Rinklebe, J.: Mercury speciation, transformation, and transportation in soils, atmospheric flux, and implications for risk management: A critical review, Environment International, 126, 747-761, 10.1016/j.envint.2019.03.019, 2019.
Obrist, D., Faïn, X., and Berger, C.: Gaseous elemental mercury emissions and CO(2) respiration rates in terrestrial soils under controlled aerobic and anaerobic laboratory conditions, Science of the Total Environment, 408, 1691-1700, 2010.
Obrist, D.: Mercury distribution across 14 U.S. forests. Part II: Patterns of methyl mercury concentrations and areal mass of total and methyl mercury, Environmental Science & Technology, 46, 7434, 2012.
Obrist, D., Pokharel, A. K., and Moore, C.: Vertical profile measurements of soil air suggest immobilization of gaseous elemental mercury in mineral soil, Environmental Science & Technology, 48, 2242, 2014.
Obrist, D., Kirk, J. L., Zhang, L., Sunderland, E. M., Jiskra, M., and Selin, N. E.: A review of global environmental mercury processes in response to human and natural perturbations: Changes of emissions, climate, and land use, Ambio, 47, 116-140, 10.1007/s13280-017-1004-9, 2018.
Olson, C., Jiskra, M., Biester, H., Chow, J., and Obrist, D.: Mercury in Active-Layer Tundra Soils of Alaska: Concentrations, Pools, Origins, and Spatial Distribution, Global Biogeochemical Cycles, 32, 1058-1073, 10.1029/2017gb005840, 2018.
Osterwalder, S., Sommar, J., Akerblom, S., Jocher, G., Fritsche, J., Nilsson, M. B., Bishop, K., and Alewell, C.: Comparative study of elemental mercury flux measurement techniques over a Fennoscandian boreal peatland, Atmospheric Environment, 172, 16-25, 10.1016/j.atmosenv.2017.10.025, 2018.
Osterwalder, S., Huang, J.-H., Shetaya, W. H., Agnan, Y., Frossard, A., Frey, B., Alewell, C., Kretzschmar, R., Biester, H., and Obrist, D.: Mercury emission from industrially contaminated soils in relation to chemical, microbial, and meteorological factors, Environmental Pollution, 250, 944-952, 10.1016/j.envpol.2019.03.093, 2019.
Outridge, P. M., Mason, R. P., Wang, F., Guerrero, S., and Heimburger-Boavida, L. E.: Updated global and oceanic mercury budgets for the united nations global mercury assessment 2018, Environmental Science & Technology, 52, 11466-11477, 10.1021/acs.est.8b01246, 2018.
Pan, L., Lin, C.-J., Carmichael, G. R., Streets, D. G., Tang, Y., Woo, J.-H., Shetty, S. K., Chu, H.-W., Ho, T. C., Friedli, H. R., and Feng, X.: Study of atmospheric mercury budget in East Asia using STEM-Hg modeling system, Science of the Total Environment, 408, 3277-3291,

10.1016/j.scitotenv.2010.04.039, 2010.
Pannu, R., Siciliano, S. D., and O'Driscoll, N. J.: Quantifying the effects of soil temperature, moisture and sterilization on elemental mercury formation in boreal soils, Environmental Pollution, 193, 138, 2014.
Peleg, M., Tas, E., Matveev, V., Obrist, D., Moore, C. W., Gabay, M., and Luria, M.: Observational evidence for involvement of nitrate radicals in nighttime oxidation of mercury, Environmental Science & Technology, 49, 14008, 2015.
Perez-Rodriguez, M., Biester, H., Aboal, J. R., Toro, M., and Martinez Cortizas, A.: Thawing of snow and ice caused extraordinary high and fast mercury fluxes to lake sediments in Antarctica, Geochimica Et Cosmochimica Acta, 248, 109-122, 10.1016/j.gca.2019.01.009, 2019.
Richardson, J. B., and Friedland, A. J.: Mercury in coniferous and deciduous upland forests in northern New England, USA: implications of climate change, Biogeosciences, 12, 6737-6749, 10.5194/bg-12-6737-2015, 2015.
Risch, M. R., DeWild, J. F., Gay, D. A., Zhang, L., Boyer, E. W., and Krabbenhoft, D. P.: Atmospheric mercury deposition to forests in the eastern USA, Environmental Pollution, 228, 8-18, 10.1016/j.envpol.2017.05.004, 2017.
Slemr, F., Weigelt, A., Ebinghaus, R., Bieser, J., Brenninkmeijer, C. A. M., Rauthe-Schoech, A., Hermann, M., Martinsson, B. G., van Velthoven, P., Boenisch, H., Neumaier, M., Zahn, A., and Ziereis, H.: Mercury distribution in the upper troposphere and lowermost stratosphere according to measurements by the IAGOS-CARIBIC observatory: 2014-2016, Atmospheric Chemistry and Physics, 18, 12329-12343, 10.5194/acp-18-12329-2018, 2018.
Sørbotten, L. E.: Hill slope unsaturated flowpaths and soil moisture variability in a forested catchment in Southwest China, MD, Department of Plant and Environmental Sciences, University of Life Sciences, 2011.
Spolaor, A., Barbaro, E., Cappelletti, D., Turetta, C., Mazzola, M., Giardi, F., Bjorkman, M. P., Lucchetta, F., Dallo, F., Pfaffhuber, K. A., Angot, H., Dommergue, A., Maturilli, M., Saiz-Lopez, A., Barbante, C., and Cairns, W. R. L.: Diurnal cycle of iodine, bromine, and mercury concentrations in Svalbard surface snow, Atmospheric Chemistry and Physics, 19, 13325-13339, 10.5194/acp-19-13325-2019, 2019.
St Louis, V. L., Graydon, J. A., Lehnherr, I., Amos, H. M., Sunderland, E. M., St Pierre, K. A., Emmerton, C. A., Sandilands, K., Tate, M., Steffen, A., and Humphreys, E. R.: Atmospheric Concentrations and Wet/Dry Loadings of Mercury at the Remote Experimental Lakes Area, Northwestern Ontario, Canada, Environmental Science & Technology, 53, 8017-8026, 10.1021/acs.est.9b01338, 2019.
Sun, T., Ma, M., Wang, X., Wang, Y., Du, H., Xiang, Y., Xu, Q., Xie, Q., and Wang, D.: Mercury transport, transformation and mass balance on a perspective of hydrological processes in a subtropical forest of China, Environmental Pollution, 254, 10.1016/j.envpol.2019.113065, 2019.
Teixeira, D. C., Lacerda, L. D., and Silva-Filho, E. V.: Foliar mercury content from tropical trees and its correlation with physiological parameters in situ, Environmental Pollution, 242, 1050-1057, 10.1016/j.envpol.2018.07.120, 2018.
Wang, Q., Luo, Y., Du, B., Ye, Z., and Duan, L.: Influencing factors of mercury emission flux from forest soil at tieshanping,chongqing, Environmental Science, 35, 1922-1927, 2014.
Wang, S., Feng, X., Qiu, G., Fu, X., and Wei, Z.: Characteristics of mercury exchange flux between soil and air in the heavily air-polluted area, eastern Guizhou, China, Atmospheric Environment, 41, 5584-5594, 2007.

745 Wang, X., Bao, Z., Lin, C.-J., Yuan, W., and Feng, X.: Assessment of global mercury deposition through
746 litterfall, Environmental science & technology, 50, 8548-8557, 2016.
747 Wang, X., Lin, C.-J., Feng, X., Yuan, W., Fu, X., Zhang, H., Wu, Q., and Wang, S.: Assessment of regional
748 mercury deposition and emission outflow in mainland China, Journal of Geophysical Research-
749 Atmospheres, 123, 9868-9890, 10.1029/2018jd028350, 2018.
750 Wang, Z., Zhang, X., Xiao, J., Zhijia, C., and Yu, P.: Mercury fluxes and pools in three subtropical
751 forested catchments, southwest China, Environmental Pollution, 157, 801-808,
752 10.1016/j.envpol.2008.11.018, 2009.
753 Wang, Z. H., Zhang, G., Wang, Y., Zhao, Y. X., and Sun, X. J.: Research on mercury flux between snow
754 and air under the condition of seasonal snow cover environment, Journal of Agro-Environment
755 Science, 32, 601-606, 2013.
756 Wright, L. P., Zhang, L., and Marsik, F. J.: Overview of mercury dry deposition, litterfall, and throughfall
757 studies, Atmospheric Chemistry and Physics, 16, 13399-13416, 10.5194/acp-16-13399-2016, 2016.
758 Wu, Z., Dai, E., Wu, Z., and Lin, M.: Future forest dynamics under climate change, land use change, and
759 harvest in subtropical forests in Southern China, Landscape Ecology, 34, 843-863, 10.1007/s10980-
760 019-00809-8, 2019.
761 Xin, M., and Gustin, M. S.: Gaseous elemental mercury exchange with low mercury containing soils:
762 Investigation of controlling factors, Applied Geochemistry, 22, 1451-1466, 2007.
763 Yu, Q., Luo, Y., Xu, G., Wu, Q., Wang, S., Hao, J., and Duan, L.: Subtropical forests act as mercury sinks
764 but as net sources of gaseous elemental mercury in south China, Environmental Science &
765 Technology, 54, 2772-2779, 10.1021/acs.est.9b06715, 2020.
766 Yuan, W., Sommar, J., Lin, C.-J., Wang, X., Li, K., Liu, Y., Zhang, H., Lu, Z., Wu, C., and Feng, X.:
767 Stable Isotope Evidence Shows Re-emission of Elemental Mercury Vapor Occurring after Reductive
768 Loss from Foliage, Environmental Science & Technology, 53, 651-660, 10.1021/acs.est.8b04865,
769 2019a.
770 Yuan, W., Wang, X., Lin, C.-J., Sommar, J., Lu, Z., and Feng, X.: Process factors driving dynamic
771 exchange of elemental mercury vapor over soil in broadleaf forest ecosystems, Atmospheric
772 Environment, 219, 10.1016/j.atmosenv.2019.117047, 2019b.
773 Zarate-Valdez, J. L., Zasoski, R. J., and Lauchli, A.: Short-term effects of moisture content on soil
774 solution pH and soil Eh, Soil Science, 171, 423-431, 10.1097/01.ss.0000222887.13383.08, 2006.
775 Zhang, G., Wang, N., Ai, J.-C., Zhang, L., Yang, J., and Liu, Z.-Q.: Characteristics of mercury exchange
776 flux between soil and atmosphere under the snow retention and snow melting control, Huan jing ke
777 xue= Huanjing kexue, 34, 468-475, 2013.
778 Zhang, H., Lindberg, S. E., Marsik, F. J., and Keeler, G. J.: Mercury air/surface exchange kinetics of
779 background soils of the tahquamenon river watershed in the Michigan Upper Peninsula, Water Air &
780 Soil Pollution, 126, 151-169, 2001.
781 Zhang, H., Lindberg, S. E., Barnett, M. O., Vette, A. F., and Gustin, M. S.: Dynamic flux chamber
782 measurement of gaseous mercury emission fluxes over soils. Part 1: simulation of gaseous mercury
783 emissions from soils using a two-resistance exchange interface model, Atmospheric Environment,
784 36, 835-846, 2002.
785 Zhang, H., Nizzetto, L., Feng, X., Borga, K., Sommar, J., Fu, X., Zhang, H., Zhang, G., and Larssen, T.:
786 Assessing Air-Surface Exchange and Fate of Mercury in a Subtropical Forest Using a Novel Passive
787 Exchange-Meter Device, Environmental Science & Technology, 53, 4869-4879,
788 10.1021/acs.est.8b06343, 2019a.

Zhang, L., Zhou, P., Cao, S., and Zhao, Y.: Atmospheric mercury deposition over the land surfaces and the associated uncertainties in observations and simulations: a critical review, Atmospheric Chemistry and Physics, 19, 15587-15608, 10.5194/acp-19-15587-2019, 2019b.

Zhang, Q., Huang, J., Wang, F., Mark, L., Xu, J., Armstrong, D., Li, C., Zhang, Y., and Kang, S.: Mercury distribution and deposition in glacier snow over western China, Environmental science & technology, 46, 5404, 2012.

Zhou, J., Wang, Z., Zhang, X., and Chen, J.: Distribution and elevated soil pools of mercury in an acidic subtropical forest of southwestern China, Environmental Pollution, 202, 187-195, 10.1016/j.envpol.2015.03.021, 2015.

Zhou, J., Wang, Z., Sun, T., Zhang, H., and Zhang, X.: Mercury in terrestrial forested systems with highly elevated mercury deposition in southwestern China: The risk to insects and potential release from wildfires, Environmental Pollution, 212, 188-196, 10.1016/j.envpol.2016.01.003, 2016.

Zhou, J., Wang, Z., Zhang, X., and Gao, Y.: Mercury concentrations and pools in four adjacent coniferous and deciduous upland forests in Beijing, China, Journal of Geophysical Research: Biogeosciences, 122, 1260-1274, 2017a.

Zhou, J., Wang, Z., Zhang, X., and Sun, T.: Investigation of factors affecting mercury emission from subtropical forest soil: A field controlled study in southwestern China, Journal of Geochemical Exploration, 176, 128-135, 10.1016/j.gexplo.2015.10.007, 2017b.

Zhou, J., Wang, Z., and Zhang, X.: Deposition and fate of mercury in litterfall, litter, and soil in coniferous and broad-leaved forests, Journal of Geophysical Research: Biogeosciences, 123, 2590-2603, 10.1029/2018jg004415, 2018.

Zhou, J., Du, B., Shang, L., Wang, Z., Cui, H., Fan, X., and Zhou, J.: Mercury fluxes, budgets, and pools in forest ecosystems of China: A review, Critical Reviews in Environmental Science and Technology, 50, 1411-1450, 2020.

Zhou, J., Wang, Z., Zhang, X., and Driscoll, C. T.: Measurement of vertical distribution of gaseous elemental mercury concentration in soil pore air at subtropical and temperate forests, in review.

Zhu, W., Lin, C. J., Wang, X., Sommar, J., Fu, X., and Feng, X.: Global observations and modeling of atmosphere-surface exchange of elemental mercury: a critical review, Atmospheric Chemistry & Physics, 16, 4451-4480, 2016.

Table 1. Locations and summary of measurements (mean ± standard deviation) of soil-air TGM fluxes and environmental parameters at ten plots at the subtropical and temperate forests.

Forest	Plots	Locations	Flux (ng m^{-2} hr^{-1})	Soil surface TGM (ng m^{-3})	Soil Hg concentration (ng g^{-1})	SOM (0-5, %)	Soil moisture (%)	Soil temperature (℃)	Solar radiation (W m^{-2})
Subtropical forest	Plot S-A	Top-slope of coniferous forest	2.8 ± 3.9	3.6±1.3	219±15	13.6	0.3±0.1	16.8±7.6	39.9±27.5
	Plot S-B	Middle-slope of coniferous forest	3.5 ± 4.2	3.8±1.3	263±22	16.3	0.4±0.1	16.9±7.7	40.2±27.5
	Plot S-C	Wetland	-0.80 ± 5.1	3.7±1.4	96±43	4.9	0.3±0.1	16.7±7.5	30.5±27.9
	Plot S-D	Broad-leaved forest	0.18 ± 4.3	3.3±1.4	156±17	8.8	0.3±0.1	16.9±7.6	20.3±27.9
	Plot S-E	Open field	24 ± 33	4.1±1.7	159±18	4.1	0.3±0.1	18.3±8.5	98.0±138.4
Temperate forest	Plot T-A	Chinese pine forest	-0.04±0.81	2.22±0.87	72±12	5.8	17.0±8.55	9.77±6.57	17.09±29.4
	Plot T-B	Larch forest	0.32±0.96	2.30±0.94	141±15	25	26.3±6.51	10.0±6.23	22.9±18.6
	Plot T-C	Wetland	3.81±0.52	2.47±0.92	156±21	47	42.9±8.22	10.0±6.55	22.1±19.4
	Plot T-D	Mixed broad-leaved forest	0.68±1.01	2.37±0.87	74±9	16	25.4±7.32	9.86±6.26	25.9±18.6
	Plot T-E	Open field	1.82±0.79	1.98±0.79	52±4	12	27.9±5.56	10.1±6.47	47.1±29.4

822

823 **Figure captions:**

824 **Fig. 1.** Location of the five sampling plots and the estimation of soil-air fluxes (SA fluxes, values
825 as g m^{-2} yr^{-1}) at the temperate and subtropical forest. Potential vegetation of China is from the
826 Vegetation Map of China (Hou, 1982). Up and down arrows represent emission and deposition,
827 respectively.

828 **Fig. 2.** Mean and standard deviations of soil-air TGM fluxes at the five plots for the four seasons
829 and annual values during the study at the subtropical forest (A) and temperate forest (B). The
830 number of flux observations in spring, summer, autumn and winter were 62, 92, 66 and 43 at the
831 subtropical forest and 60, 58, 60 and 14 for the temperate forest, respectively.

832 **Fig. 3.** Daily (average flux of day and night) composite Hg flux, solar radiation and soil temperature
833 at Masson pine forests plots ((A) and (B)), wetland (C), evergreen broad-leaved forest (D) and
834 open field (E) plots at the subtropical forest. The vertical arrows represent precipitation events.

835 **Fig. 4.** Daily (average flux of day and night) composite Hg flux, solar radiation and soil temperature
836 at Chinese pine forest (A), larch forest (B), wetland (C), mixed broad-leaved forest (D) and open
837 field (E) plots at the temperate forest. The vertical arrows represent precipitation events.

838 **Fig. 5.** Interplays of environmental factors on air-soil TGM exchange flux obtained by structural
839 equation model (SEM) in the temperate (a) and subtropical (b) forests.

840 **Fig. 6.** Correlation between the air TGM concentration and air-surface Hg flux measured in daytime
841 and night over four seasons for at Masson pine forest plots ((A) and (B)), wetland (C), evergreen
842 broad-leaved forest (D) and open field (E) plots at the subtropical forest.

843 **Fig. 7.** Correlation between the air TGM concentration and air-surface Hg flux measured in daytime
844 and night over four seasons for the five plots at Chinese pine forest (a), larch forest (b), wetland
845 (c), mixed broad-leaved forest (d) and open field (e) plots at the temperate forest.

846 **Fig. 8.** Diurnal patterns of soil Hg fluxes with meteorological parameters in spring (a), summer (b),
847 autumn (c) and winter (d) at the coniferous forest of the subtropical forest.

848 **Fig. 9.** Diurnal patterns of soil Hg fluxes with meteorological parameters in spring (a), summer (b),
849 autumn (c) and winter (d) at the deciduous broad-leaved forest of the temperate forest.

850

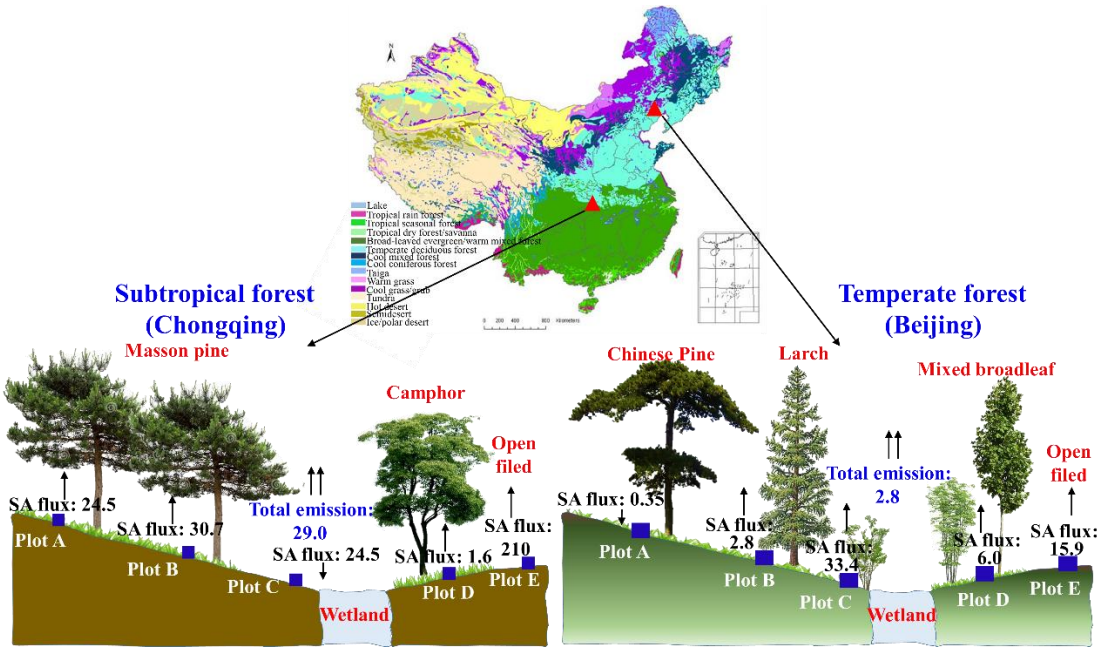

Fig. 1. Location of the five sampling plots and the estimation of soil-air fluxes (SA fluxes, values as g m^{-2} yr^{-1}) at the temperate and subtropical forest. Potential vegetation of China is from the Vegetation Map of China (Hou, 1982). Up and down arrows represent emission and deposition, respectively.

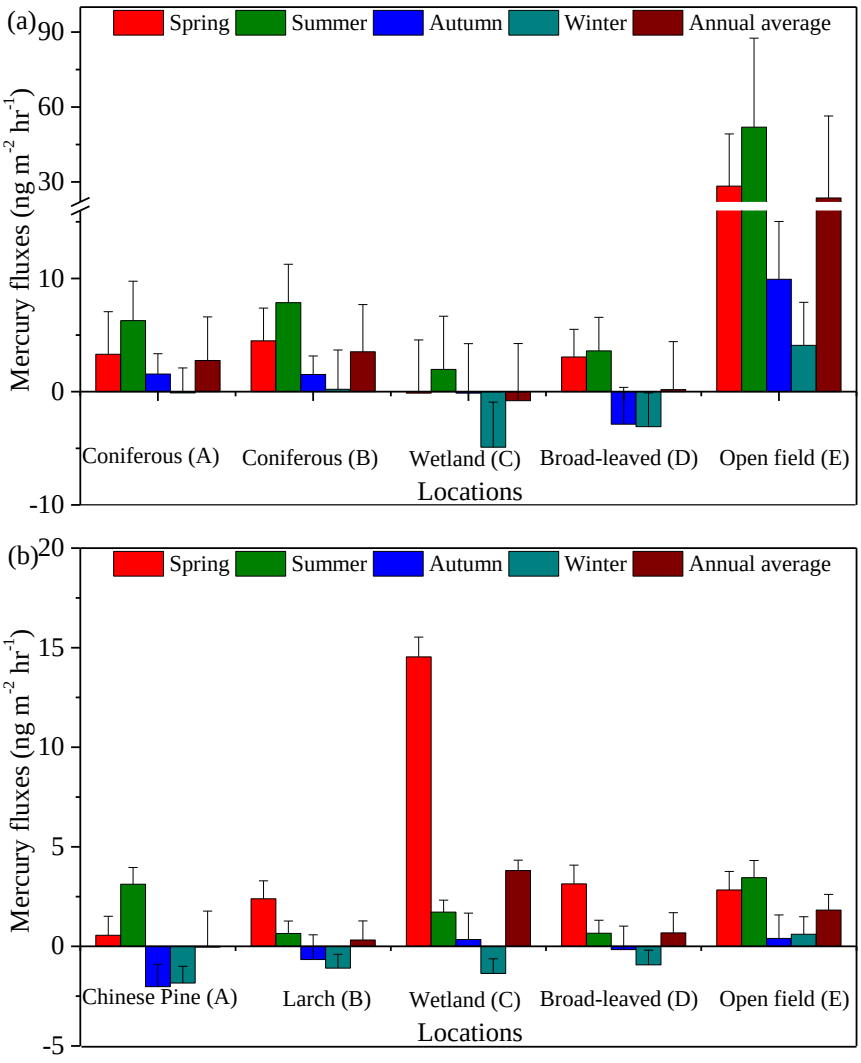

857

858

859 **Fig. 2.** Mean and standard deviations of soil-air TGM fluxes at the five plots for the four seasons
860 and annual values during the study at the subtropical forest (A) and temperate forest (B). The
861 number of flux observations in spring, summer, autumn and winter were 62, 92, 66 and 43 at the
862 subtropical forest and 60, 58, 60 and 14 for the temperate forest, respectively.

863

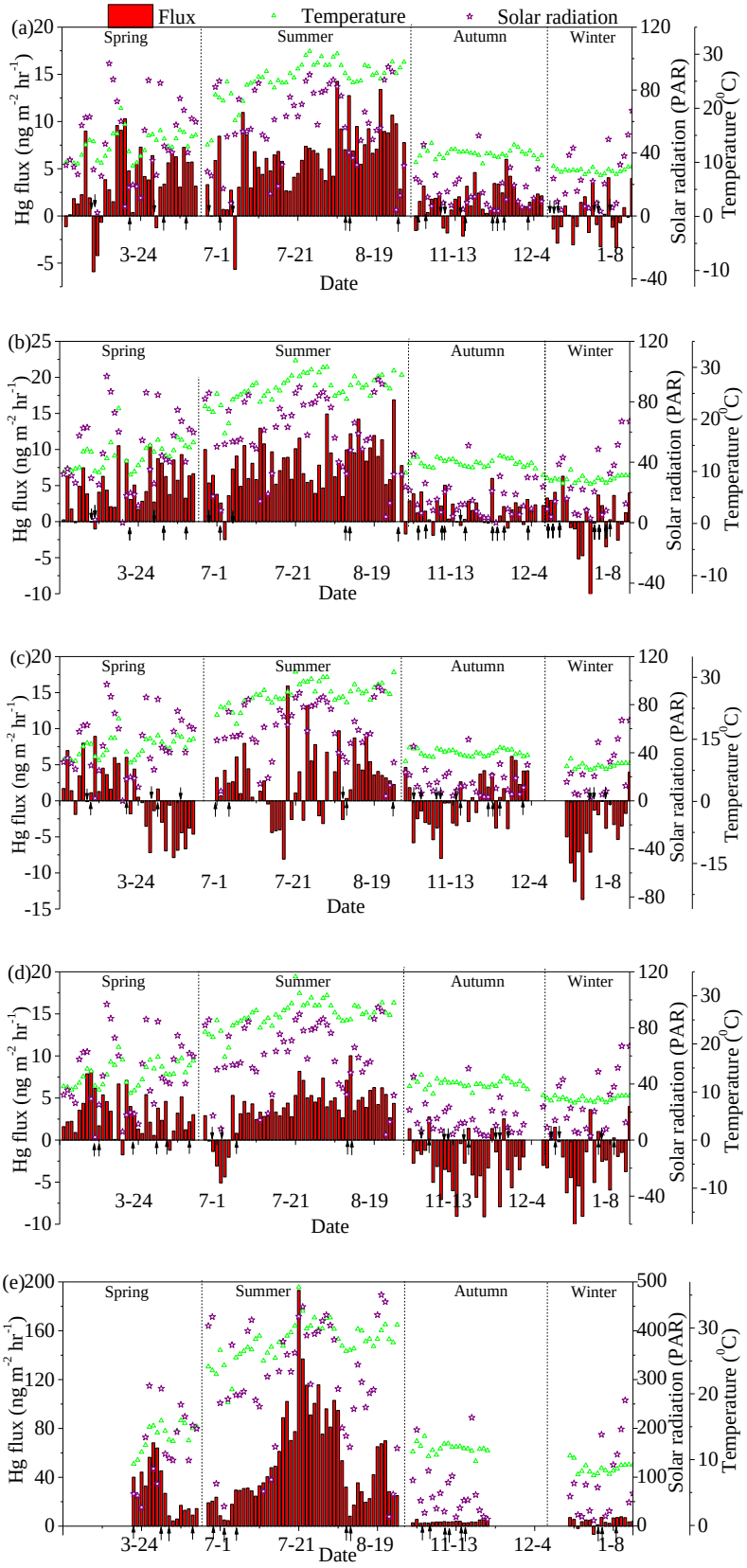

Fig. 3. Daily (average flux of day and night) composite Hg flux, solar radiation and soil temperature at Masson pine forests plots ((A) and (B)), wetland (C), evergreen broad-leaved forest (D) and open field (E) plots at the subtropical forest. The vertical arrows represent precipitation events.

873 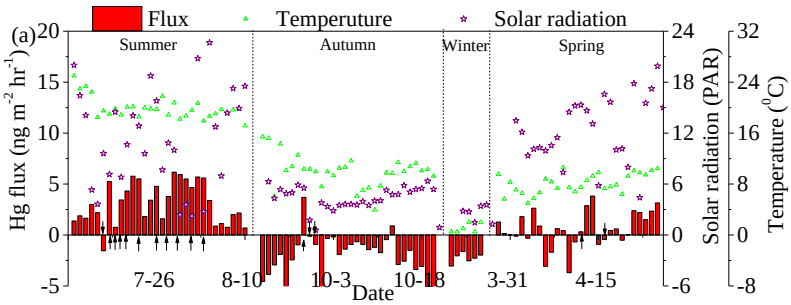

874 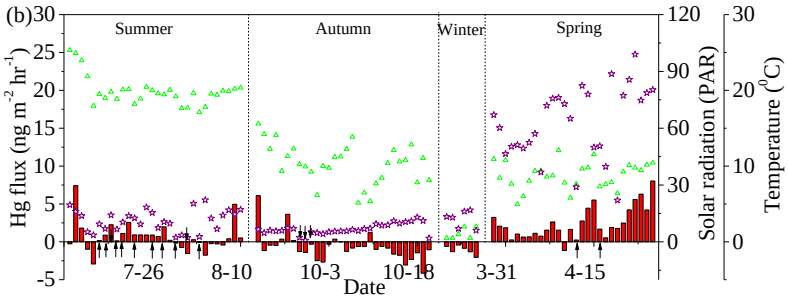

875 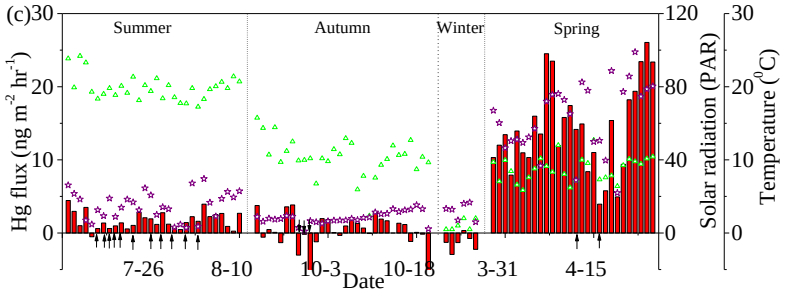

876 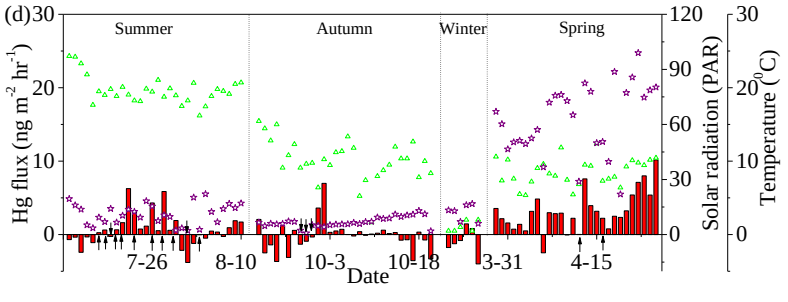

877 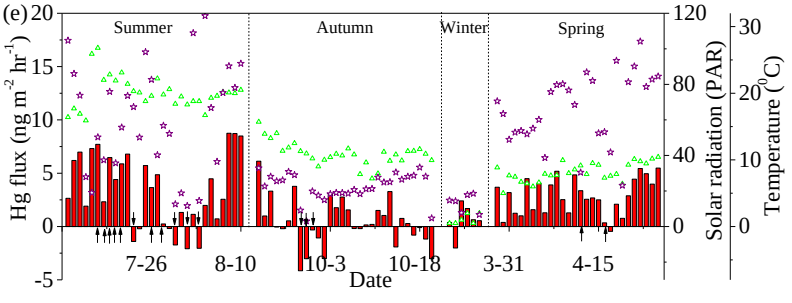

878 **Fig. 4.** Daily (average flux of day and night) composite Hg flux, solar radiation and soil temperature
879 at Chinese pine forest (A), larch forest (B), wetland (C), mixed broad-leaved forest (D) and open
880 field (E) plots at the temperate forest. The vertical arrows represent precipitation events.
881

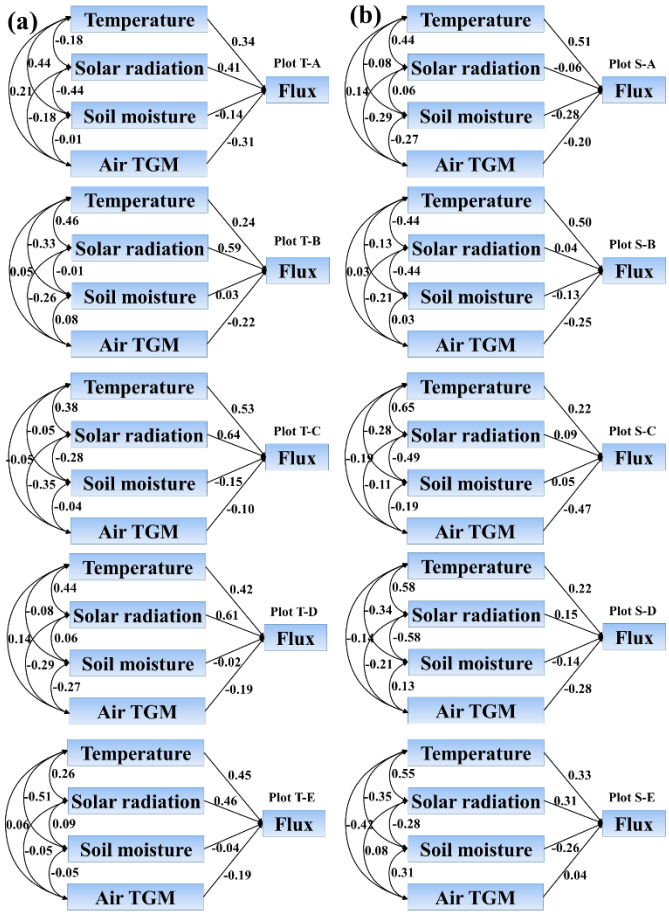

Fig. 5. Interplays of environmental factors on air-soil TGM exchange flux obtained by structural equation model (SEM) in the temperate (a) and subtropical (b) forests.

886

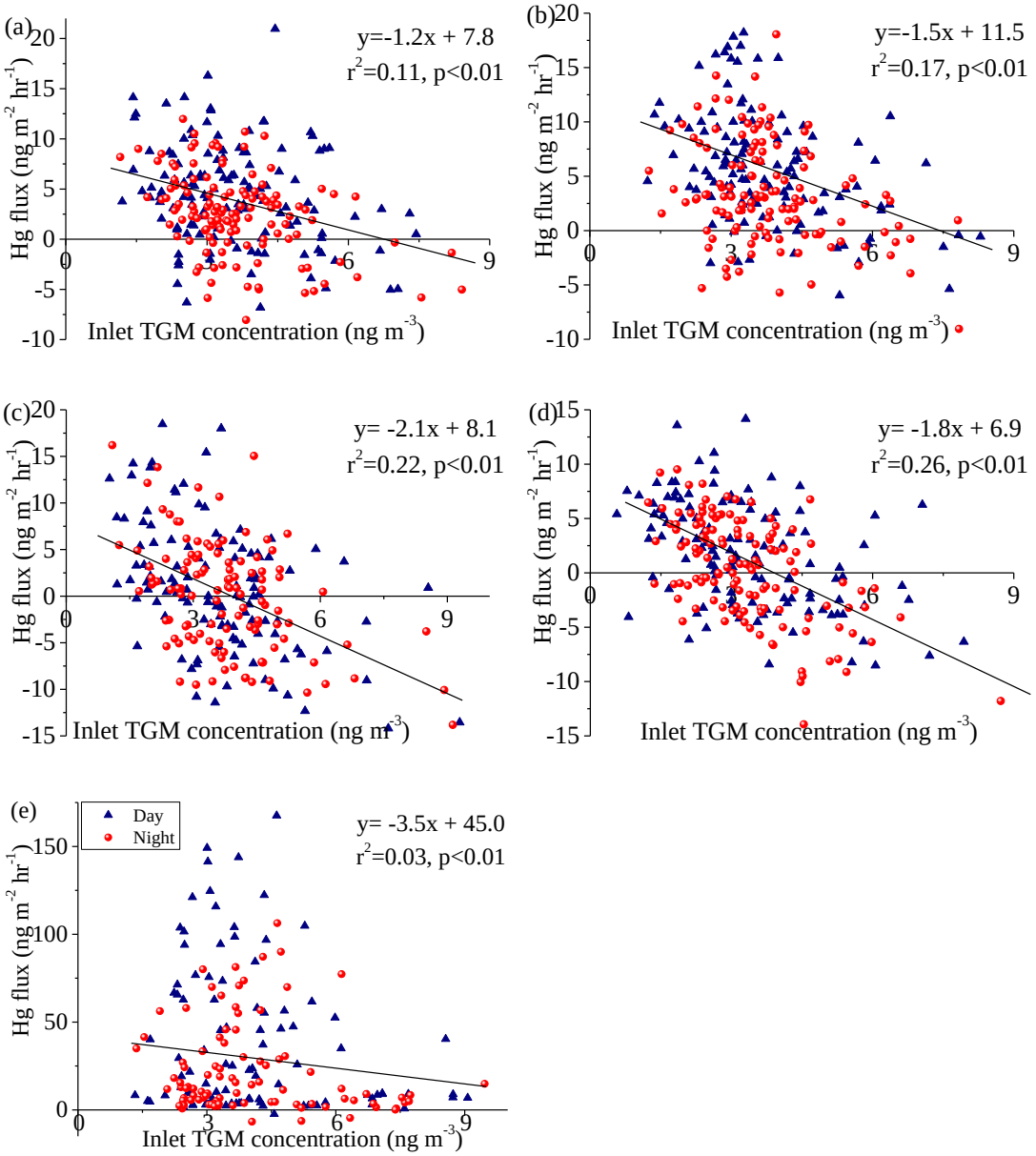

887

888

889 **Fig. 6.** Correlation between the air TGM concentration and air-surface Hg flux measured in daytime
890 and night over four seasons for at Masson pine forest plots ((A) and (B)), wetland (C), evergreen
891 broad-leaved forest (D) and open field (E) plots at the subtropical forest.

892

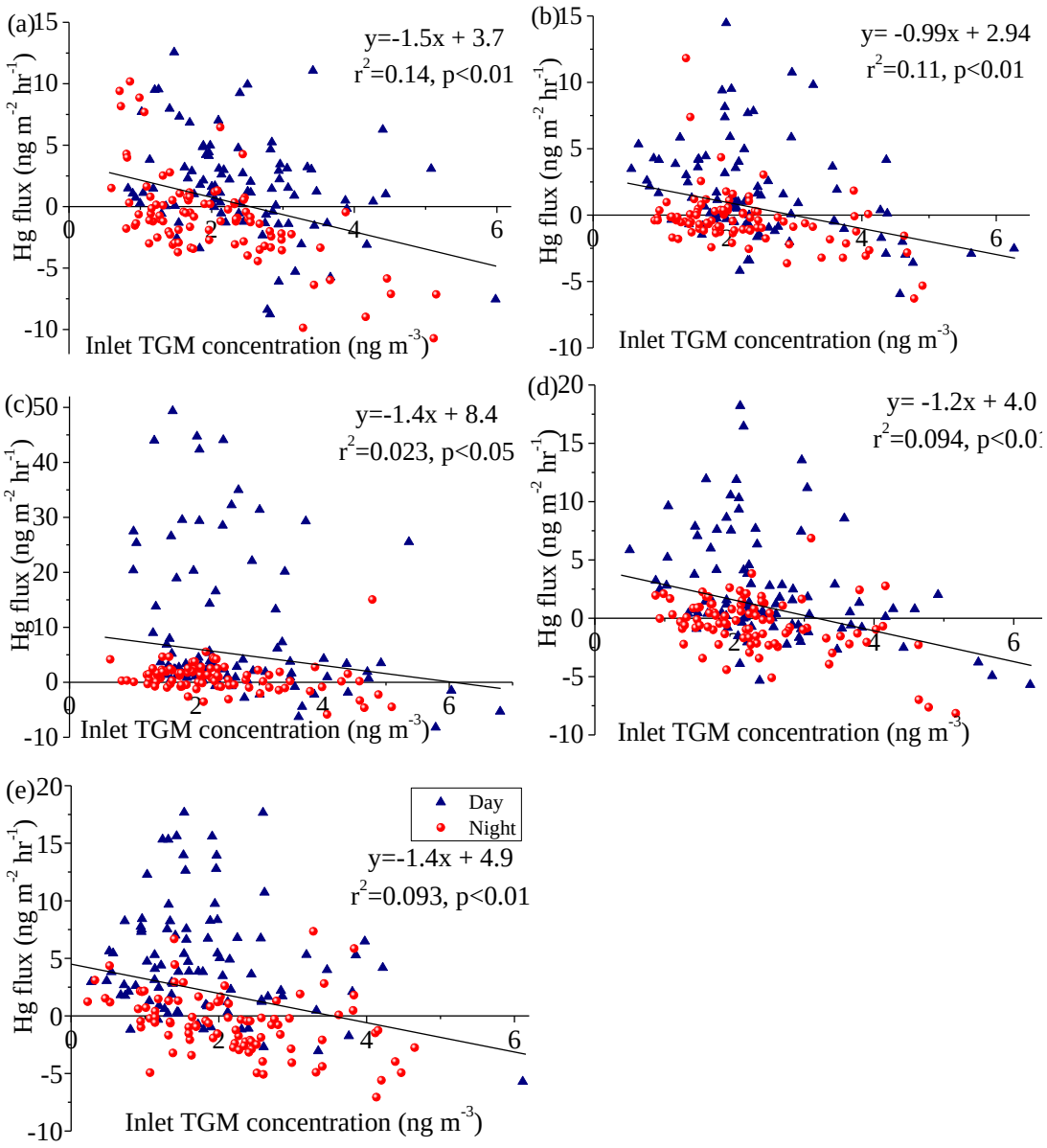

Fig. 7. Correlation between the air TGM concentration and air-surface Hg flux measured in daytime and night over four seasons for the five plots at Chinese pine forest (a), larch forest (b), wetland (c), mixed broad-leaved forest (d) and open field (e) plots at the temperate forest.

900

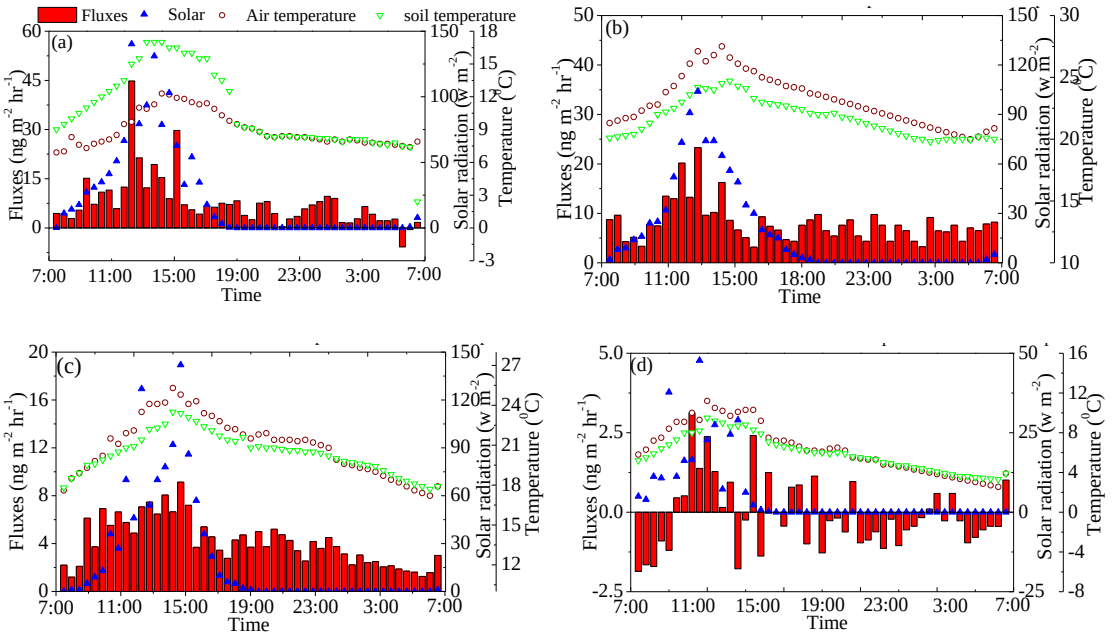

901

902 **Fig. 8.** Diurnal patterns of soil Hg fluxes with meteorological parameters in spring (a), summer (b),
903 autumn (c) and winter (d) at the coniferous forest of the subtropical forest.

904

905

906

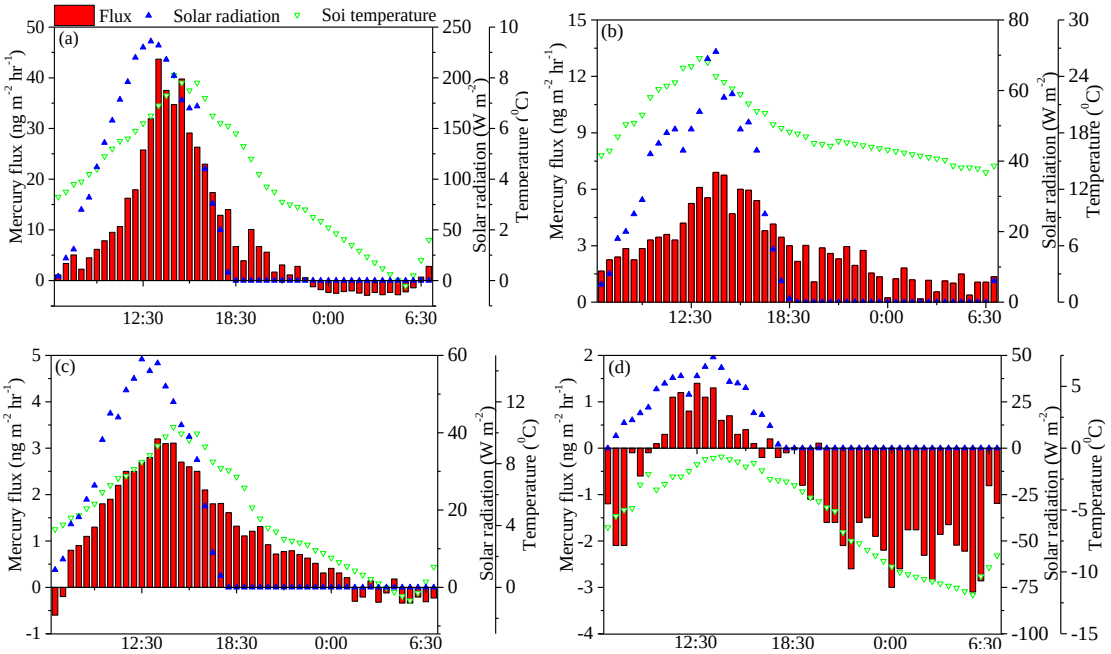

907

908 **Fig. 9.** Diurnal patterns of soil Hg fluxes with meteorological parameters in spring (a), summer (b),
909 autumn (c) and winter (d) at the deciduous broad-leaved forest of the temperate forest.

910